# Chitinase-like protein promotes tumorigenesis through disruption of cell polarity via enlarged vesicles.

Dilan Khalili[1], Martin Kunc[1], Sarah Herbrich[1], Anna M. Müller[1] and Ulrich Theopold[1]

[1] Department of Molecular Biosciences, The Wenner-Gren Institute (MBW), Stockholm University, 10691 Stockholm, Sweden

Ulrich Theopold, Department of Molecular Biosciences, The Wenner-Gren Institute (MBW),

Stockholm University, Svante Arrheniusväg 20c, 10691 Stockholm, Sweden

Phone: +46-8-164181

Email: uli.theopold@su.se

## Abstract:

Chitinase-like proteins (CLPs) are associated with tissue-remodelling and inflammation but also with several disorders, including fibrosis, atherosclerosis, allergies, and cancer. However, the CLP's role in tumors is far from clear. Here, we utilize *Drosophila melanogaster* to investigate the function of CLPs (imaginal disc growth factors; Idgf's) in $Ras^{V12}$ dysplastic salivary glands (SGs). We find one of the Idgf's members, *Idgf3,* to be transcriptionally induced in a tissue- and cell-autonomously manner in a *Drosophila* hypertrophic model for early tumor progression. Induction involves non-canonical JNK-signaling via a positive feedback loop mediated by reactive oxygen species (ROS). Moreover, Idgf3 accumulates in enlarged vesicles (EnVs) that promote tumor progression by disrupting cytoskeletal organization, independent of Rab5 and Rab11. The process is mediated via Rac1 and the downstream component, αSpectrin, which localizes to the EnVs. Similar to Idgf3, expression of two human members of the CLP family in *Drosophila* SGs aggravates tumor-related phenotypes. Our data provide new insight into a phylogenetically conserved tissue-autonomous CLP function in tumors and identify specific targets for tumor control.

## Introduction:

Chitinase-like protein (CLPs), including human Ch3L2 (YKL-39) and Ch3L1 (YKL-40) are released in various inflammatory conditions, including tumors. These proteins are secreted amongst others by immune cells, are often associated with a poor prognosis, and may promote tumor growth through interaction with the tumor microenvironment (Roslind and Johansen 2009, Shao, Hamel et al. 2009). CLPs are upregulated in patients with ductal tumors, including tumors in the lung, the breast and the pancreas (Johansen, Jensen et al. 2006, Uhlen, Zhang et al. 2017).

The discovery of the human Rat sarcoma (Ras) oncogene more than 40 years ago has led to a substantial improvement of our understanding of cancer biology. The oncogene is mutated or dysregulated in a large number of non-physiological contexts, including pancreatitis

(Fernandez-Medarde, De Las Rivas et al. 2021). Pancreatitis is characterized by inflammation, death-signaling, fibrosis, loss of cell polarity, immune cell recruitment, and obstruction of pancreatic ducts mediated via *KRAS* (Pinho, Chantrill et al. 2014). However, the causal connection between CLPs' function and tumor progression is only partially elucidated (Park, Yun et al. 2020).

Animal models have been increasingly used in molecular oncology. This includes the fruitfly *Drosophila melanogaster*, where overexpression of dominant-active Ras ($Ras^{V12}$) in proliferating tissue leads to benign tumors, simultaneous reduction of cell polarity genes and to progression towards an invasive stage. (Brumby and Richardson 2003, Pagliarini and Xu 2003, Igaki, Pagliarini et al. 2006, Perez, Lindblad et al. 2017). Central to this switch is the C-Jun N-terminal kinase (JNK) - signaling pathway, which can become activated via loss of cell polarity and promotes tumor growth (Zhu, Xin et al. 2010). However, the outcome of activated JNK is mediated in a context-dependent manner due to downstream effects, several of which are yet to be elucidated (Ciapponi, Jackson et al. 2001, Zeke, Misheva et al. 2016). Among potential JNK regulators, spectrin family members belong to cytoskeletal proteins which form a spectrin-based membrane skeleton (SBMS) (Bennett and Baines 2001). Through the Rac family of small GTPases, cell polarity and SBMS organization are maintained (Lee and Thomas 2011, Fletcher, Elbediwy et al. 2015). Although the exact relationship between Spectrin and JNK in tumors remains to be established, Rac1 cooperates with JNK in tissue growth (Baek, Kwon et al. 2010, Wertheimer, Gutierrez-Uzquiza et al. 2012, Archibald, Mihai et al. 2015).

To explore the tissue autonomous function of CLPs in a ductal tumor, we utilize the *Drosophila melanogaster* salivary glands (SGs) - like the pancreas a terminally differentiated secretory organ. Generally, *Drosophila* CLPs are endogenously expressed in the larvae and include six members, termed Idgf 1-6 (Imaginal disc growth factors), which are involved in wound healing and restoration of cell organization (Kirkpatrick, Matico et al. 1995, Kawamura, Shibata et al. 1999, Kucerova, Kubrak et al. 2016, Yadav and Eleftherianos 2018). The SGs epithelial luminal organization and the conserved activation of the tumor-promoting signaling factors make them suitable for dissecting CLP's tissue autonomous function. Moreover, the lumen separating a single layer of cells can be disrupted by constitutive active *Drosophila Ras* ($Ras^{V12}$) (Krautz, Khalili et al. 2020).

Here we investigated the role of *Drosophila* Idgf's in $Ras^{V12}$ SGs. We show that one of the CLP's members, *Idgf3*, is induced cell-autonomously, leading to a partial loss of epithelial polarity and decrease of the SG lumen. This involves induction of non-canonical JNK-signaling that regulates *Idgf3* independently of the downstream transcription factor Jun and Fos. Instead, ROS production via JNK promotes induction of *Idgf3*, creating a tumor-promoting signaling loop. Idgf3 through Rac1 promotes the formation of enlarged vesicles (EnVs) via αSpectrin. Inhibiting EnV formation by knocking-down *Idgf3* and the downstream factor, *αSpectrin,* restores cell organization. Similar to Idgf3, overexpression of two human CLPs in Drosophila $Ras^{V12}$ SGs, aggravates hyperplasia and leads to EnV formation for one human CLP. Thus, our work signifies the evolutionary conserved importance of tumor-induced CLP's in the cell-autonomous dysregulation of ductal organs.

## Results

### Idgf3 promotes a dysplastic phenotype

Obstruction of the SG lumen by the constitutive-active oncogene, *Ras*$^{V12}$, under the *Beadex-Gal4* driver (denoted as *Ras*$^{V12}$) disrupts organ function between 96 h and 120 h after egg desposition (AED) (Khalili, Kalcher et al. 2021). Being that CLPs have been implicated in the loss of cell polarity (Morera, Steinhauser et al. 2019), we investigated whether *Drosophila* CLPs contribute to this phenotype. In order to find out whether CLPs were induced in *Ras*$^{V12}$ glands, we assessed relative mRNA levels at two different time points, 96 h and 120h AED. Only one of the *CLP* members, namely *Idgf3,* was significantly upregulated at both time points (Fig. 1B and Fig. S1A ). Therefore, we decided to focus on *Idgf3's* effects on dysplastic glands.

To characterize the spatial and temporal expression of *Idgf3* we performed in situ hybridization (ISH) using Idgf3-*specific* probes. In SGs of *w*$^{1118}$ *(*denoted as *WT)* larvae, *Idgf3* was expressed in the most proximal part (PP) confirming earlier results (Fig. S1B at 96 h, (Kawamura, Shibata et al. 1999)). In line with qPCR data (Fig. S1A), a higher level of *Idgf3* was detected in *Ras*$^{V12}$ SGs (Fig. S1C). At 120 h, we still observed *Idgf3* in the PP of *WT* glands, while in *Ras*$^{V12}$ larvae, the signal was again substantially stronger and detected throughout the whole gland (Fig. S1D-E).

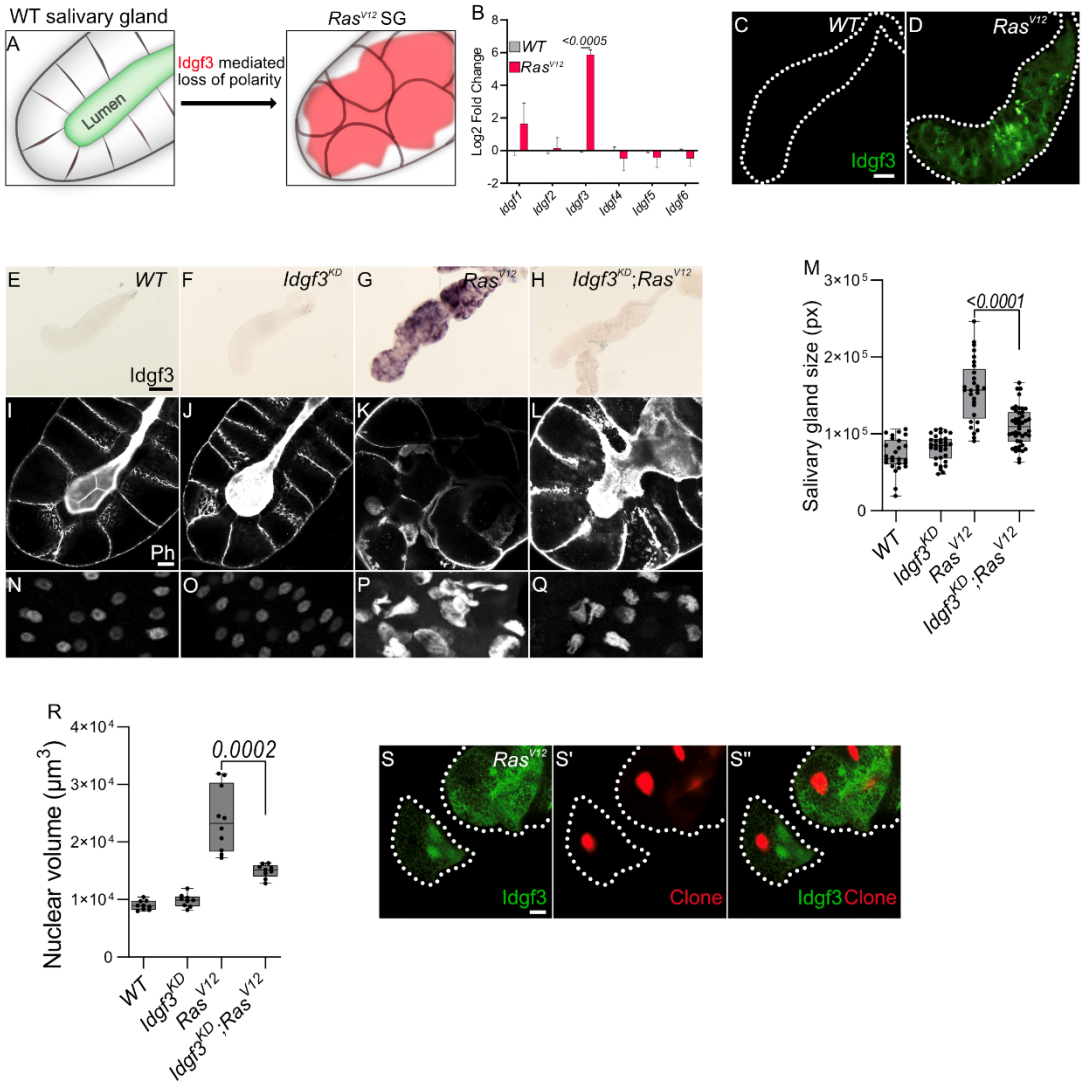


**Figure 1 Idgf3 promotes growth and disrupts tissue architecture in a cell-autonomous manner**

(A) Idfg3 drives dysplasia upon oncogene, *Ras$^{V12}$*, overexpression.
(B) qPCR data showing induction of *Idgf3* in 120 h AED *Ras$^{V12}$* glands.
(C-D) Idgf3 tagged with GFP was localized in the dysplastic glands.
(E-H) Knock-down of *Idgf3* in *Ras$^{V12}$* glands confirmed reduced mRNA levels as shown with in situ hybridization.
(I-L) F-actin (Phalloidin) staining revealed partial restoration of the lumen in *Idgf3-KD;Ras$^{V12}$* glands, in comparison to *Ras$^{V12}$* alone.
(M) SG size quantification showing a reduction in tissue size in *Idgf3-KD;Ras$^{V12}$* SG compared to *Ras$^{V12}$* alone.
(N-Q) Nuclei in DAPI stained SG displayed a reduced size in *Idgf3-KD;Ras$^{V12}$*.
(R) Nuclear quantification showing nuclear volume in the indicated genotypes.
(S-S'') SG *Ras$^{V12}$*clones displaying strong Idgf3::GFP signal.
Scale bars in (C-D) represent 100 $\mu$m (E-H), 0.3 mm and (I-L, S-S'') 20 $\mu$m. Data in (B) represent 3 independent replicas summarized as mean ± SD. Boxplot in (M) represent at least 20 SG pairs and (R) represent 10 SG pairs. Whisker length min to max, bar represent median. P-value quantified with Student's t-test.

Idgf3 contains an N-terminal signal peptide and has been detected in hemolymph (Karlsson, Korayem et al. 2004). To analyze its subcellular tissue distribution in SGs, we used a C-terminally GFP-tagged version of Idgf3 (Kucerova, Kubrak et al. 2016). At 96 h we could not detect Idgf3 in the whole *WT* or *Ras*$^{V12}$ animals (Fig. S1F-G'), possibly due to limited sensitivity. Likewise, 120 h old *WT* larvae did not show any detectable signal (Fig. S1H-H') while a strong Idgf3 signal was detected in *Ras*$^{V12}$ SGs (FigS1I-I'). To better understand Idgf3 distribution at a higher resolution, we dissected 120 h AED glands. *WT* glands had a weaker Idgf3::GFP signal in comparison to the *Ras*$^{V12}$ (Fig. 1C-D). Moreover, Idgf3 was unevenly distributed throughout *Ras*$^{V12}$ SGs (Fig. 1D).

The increased level of *Idgf3* between 96 h and 120 h strongly correlated with loss of tissue- and cell-organization and an increased nuclear volume. In order to characterize the role of Idgf3 in *Ras*$^{V12}$ glands, we used a specific *Idgf3 RNA-interference* (*RNAi*, denoted as *KD*). We focused on 120 h larvae, unless otherwise stated, since they showed the most robust dysplastic phenotype. Efficient knockdown of *Idgf3* was confirmed using ISH and at protein level (Fig 1E-H, S1J-M; quantified in N, (Kucerova, Kubrak et al. 2016)). Macroscopic inspection showed that *Idgf-KD;Ras*$^{V12}$ SGs were smaller than *Ras*$^{V12}$ SGs (Fig 1G-H, quantified in Fig 1M), thus resembling WT controls. To gain insight into the cellular organization, we stained the glands for F-actin (Phalloidin: Ph) and DNA using DAPI. In *Idgf-KD* the cells retained their cuboidal structure, and the lumen was visible as in *WT*, indicating that Idgf3 on its own does not affect cellular architecture (Fig. 1I-J). In contrast, in *Ras*$^{V12}$ glands cellular architecture was lost, and the lumen was absent (Fig. 1K, (Khalili, Kalcher et al. 2021). In *Idgf-KD;Ras*$^{V12}$ SGs a reversal to the normal distribution of F-actin and partial restoration of the lumen was observed (Fig 1 L). Similarly, the nuclear volume, which increased in *Ras*$^{V12}$ SGs returned to near wild type levels upon *Idgf3-KD* (Fig. 1 N-Q, quantified in Fig 1R). This indicates that *Idgf3-KD* can rescue Ras$^{V12}$-induced dysplasia.

In order to unravel the specific effects mediated by Idgf3 we further investigated *Ras*$^{V12}$ associated phenotypes, including fibrosis and the cellular immune response. As recently reported, *Ras*$^{V12}$ SGs displayed increased levels of the extracellular matrix components (ECM), including collagen IV and SPARC (BM40, (Khalili, Kalcher et al. 2021)). *Idgf-KD* alone did not affect SPARC levels in comparison to the *WT* (Fig. S1 O-P) but *Idgf-KD;Ras*$^{V12}$ SGs displayed significantly reduced SPARC levels in comparison to *Ras*$^{V12}$ (Fig. S1 Q-R, quantified in S). To assess whether this led to a reduced inflammatory responses, we examined the recruitment of plasmatocytes, macrophage-like cells previously reported to be recruited towards tumors (Perez, Lindblad et al. 2017). We found that both control and *Idgf-KD* glands did not show recruitment of hemocytes (Fig. S1T-U). In contrast to the effects on ECM components, *Idgf3-KD* in *Ras*$^{V12}$ glands did not lead to any changes in hemocyte attachment (Fig. S1V-W, quantified in X).

Finally, to assess whether Idgf3::GFP was induced cell-autonomously, we generated clones expressing *Ras*$^{V12}$ and nuclear *red fluoresent protein* (*RFP*) through a *heat-shock* driver. We found that Idgf3::GFP was expressed in the clonal tumor cells, whereas the WT cells were devoided of Idgf3::GFP (Fig. 1 S).

Taken together, upon *Ras*$^{V12}$ overexpression, *Idgf3* is induced cell-autonomously and promotes SG overgrowth, loss of cell organization, and fibrotic-like accumulation of the ECM, but not immune cell recruitment.

**Idgf3 induces dysplasia via a non-canonical JNK-pathway**

Dysplasia is driven by internal and external factors that work either in concert or independently. Similar to what we observed in *Idgf3-KD;Ras*$^{V12}$ glands, blocking the sole *Drosophila* JNK member *basket* reverts several tumour phenotypes. Moreover, the dysplastic loss of apical and basolateral polarity between 96 h and 120 h is driven by the JNK-pathway (Fig. 2A, (Krautz, Khalili et al. 2020)). The time frame in which we observed upregulation of *Idgf3* coincided with the period during which blocked JNK restored tissue organization and homeostasis, similar to what occurs in *Idgf-KD;Ras*$^{V12}$ SGs (Fig. 1L, S1R). Therefore, we sought to determine the role of JNK-signaling in the regulation of Idgf3.

First, we performed a targeted JNK RNAi-screen using Idgf3::GFP intensity in the glands as a readout for KD of JNK signaling components. We confirmed the sensitivity of the Idgf3::GFP construct by *Idgf3-KD* in *Ras*$^{V12}$ SGs compared to *Ras*$^{V12}$ glands (Fig. S2A-B, quantified in Fig S2L). KD of the two classical TNF receptors upstream of JNK, *Grnd* (*Grindelwald*) and *Wgn* (*Wengen*) similarly reduced Idgf3::GFP intensity (Fig 2C-D, quantified in F, S2A-L; for the complete screen, (Palmerini, Monzani et al. 2021)). A similar effect was observed upon suppression of *dTAK,* a downstream component of Grnd/Wgn, in *Ras*$^{V12}$ glands (Fig S2A, E, quantified in L). Furthermore, suppressing JNK using a dominant-negative version *(JNK*$^{DN}$*)* displayed the strongest reduction of the Idgf3::GFP signal (Fig 2SA, F, quantified in L). Similar effects were observed with *JNK-KD* (Fig. 2B, E, quantified in F). In contrast suppression of the two transcription factors that form the AP1 complex downstream of JNK using dominant-negative variants Jun (*Jun*$^{DN}$) and Fos (*Fos*$^{DN}$) (Perkins, Dailey et al. 1988) did not have any effect (Fig. S2I-J, quantified in L). In agreement, *Jun*$^{DN}$ and *Fos*$^{DN}$ did not reduce phospho-JNK (pJNK) levels, although *Fos*$^{DN}$ reduced the activity of the JNK-reporter construct to some extent (TRE.GFP, Fig. S2M-R', quantified in S and T). Altogether this suggests that Idgf3 protein levels are regulated downstream of JNK either independently of transcriptional regulation through JUN/FOS or in a redundant manner.

To further characterize Idgf3 regulation, we asked whether the reduction of Idgf3::GFP intensity was due to transcriptional regulation. ISH revealed a substantial reduction of endogenous *Idgf3* transcript levels in *JNK*$^{KD}$*;Ras*$^{V12}$ (Fig. 2G-H) glands, and a weaker signal in *JNK*$^{DN}$*;;Ras*$^{V12}$ (Fig. S2U-X) SGs, which was also confirmed using qPCR (Fig. S2Y).

Having observed that *Idgf3* transcript levels were not affected by *Grnd-KD* or *Wgn-KD* (Fig. 2G-I), we further investigated their involvement in activation of the JNK pathway in SGs. Using an anti-JNK phosphorylation antibody and the JNK reporter construct as readouts, the signal was significantly reduced in *Grnd-KD* and *Wgn-KD*, in comparison to *WT* glands (Fig. 2K-M', quantified in Q, R). However, in contrast to *Ras*$^{V12}$ SGs, *Grnd-KD* did not reduce pJNK signaling, and *Wgn-KD* led only to a slight reduction ($p < 0.029$, Fig. 2N-P', quantified in Q, R) (Kanda, Igaki et al. 2002, Andersen, Colombani et al. 2015). The TRE signal was not affected by either KD (Fig. 2D, F). We substantiated these data with qPCR, which confirmed efficient

KD of *Grnd* and *Wgn* in *Grnd-KD;Ras*$^{V12}$ and *Wgn-KD;Ras*$^{V12}$, respectively. However, the levels of JNK target genes, Puc and MMP, were not affected. In line with the ISH, *Idgf3* levels did not change either (Fig. S2Z). Collectively, this suggests that in *Ras*$^{V12}$ driven dysplastic glands, Grnd and Wgn do not activate the canonical JNK-pathway. Instead, they contribute to Idgf3 regulation at the post-transcriptional level. Several scenarios could explain these observations (i) disruption of the secretory machinery may inhibit canonical JNK activation (Palmerini, Monzani et al. 2021), (ii) an alternative JNK-activating signaling pathway may be activated by *Ras*$^{V12}$ (Wu, Chen et al. 2015, Krautz, Khalili et al. 2020) or (iii) disruption of cell polarity prevents proper JNK signaling (Zhu, Xin et al. 2010).

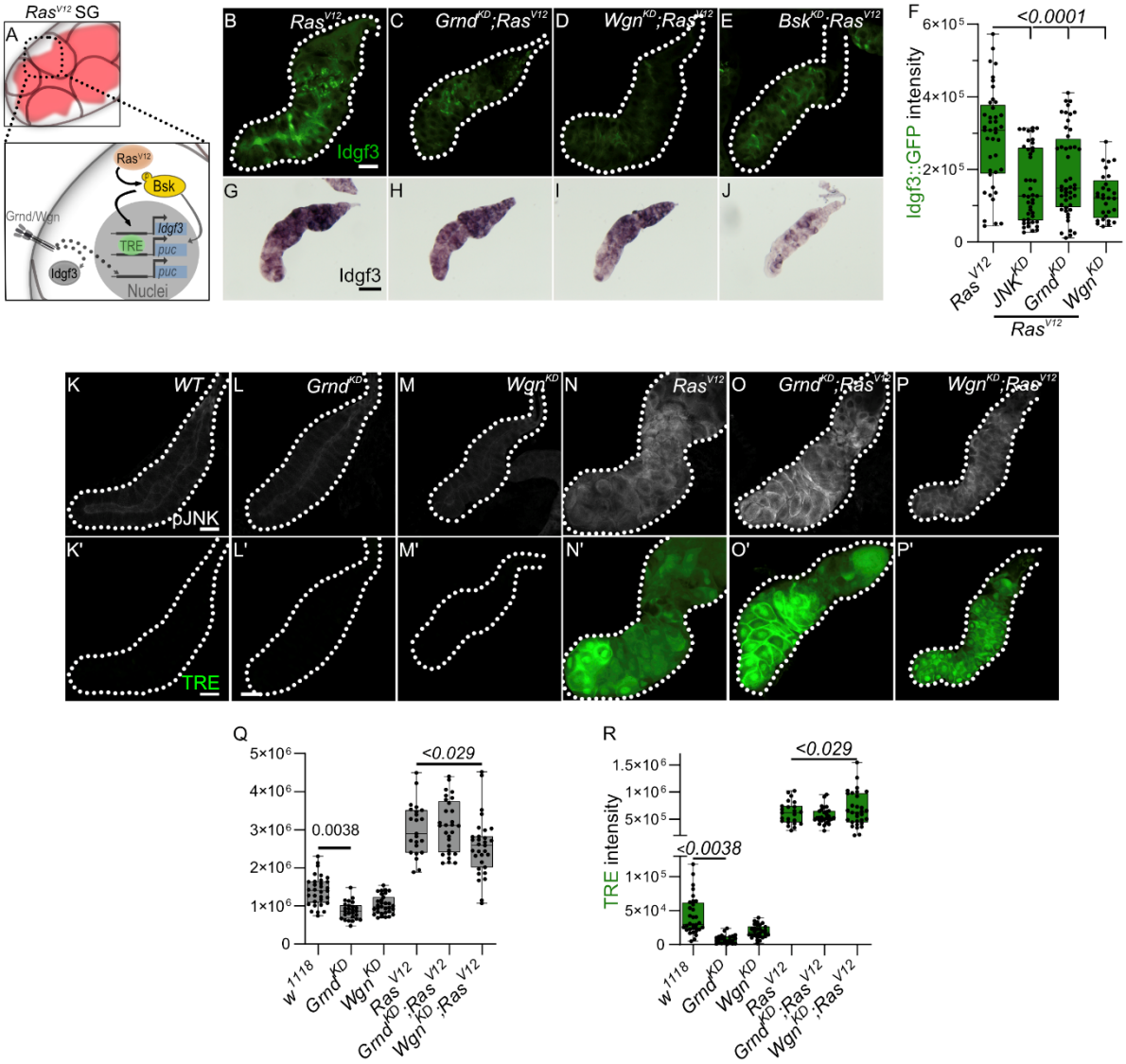


**Figure 2 Idgf3 dysplasia is mediated through JNK activity**

(A) Non-canonical JNK mediated *Idgf3* induction.

(B-E) Representative images of Idgf3::GFP in a JNK targeted screen (see Fig, S2 for the complete survey).

(F) Quantification showing Idgf3::GFP intensity was reduced by *Grnd-KD*, *Wgn-KD* and *JNK-KD* in *Ras*$^{V12}$ SG.

(G-I) *In-situ hybridization* showing reduced transcript abundance for *Idgf3* in *JNK-KD;Ras*$^{V12}$ SG.

(K-P') pJNK staining and TRE reporter construct showing non-canonical JNK signaling in *Ras*$^{V12}$ SG.
(Q-R) pJNK and TRE intensity quantification indicating strong intensity in *Grnd-KD;Ras*$^{V1}$and *Wgn-KD;Ras*$^{V1}$ glands.
Scale bars in (B-E, K-P') represent 100 $\mu$m and (G-I) 0.3 mm. Boxplot in (F,Q and R) represent at least 20 SG pairs. Whisker length min to max, bar represent median. P-value quantified with Student's t-test.

## ROS promotes *Idgf3* induction via JNK

To further dissect Idgf3 regulation, we focused on the positive JNK regulators, reactive oxygen species (ROS) both intra- and extracellularly (Diwanji and Bergmann 2017, Perez, Lindblad et al. 2017). We previously reported that ROS production in *Ras*$^{V12}$ SGs increases via JNK (Fig. 3A, (Krautz, Khalili et al. 2020)). To inhibit ROS intra- and extracellularly, we separately overexpressed the $H_2O_2$ scavengers Catalase (Cat) and a secreted form of Catalase, IRC (immune-regulated Catalase), and the $O_2^-$ scavenger SODA (Superoxide dismutase A), in the *Ras*$^{V12}$ background and quantified Idgf3::GFP intensity. Reducing levels of intracellular $H_2O_2$ (*Cat-OE*), but not $O_2^-$ (*SODA-OE*) lowered Idgf3::GFP intensity (Fig. S3A-D, quantified in S3E). Similarly, reduction of extracellular $H_2O_2$ by the secreted version of Catalase lowered Idgf3::GFP levels (Fig. 3B-E, quantified in F). Similar to the reduced tissue size and improved tissue integrity in *Idgf3-KD;;Ras*$^{V12}$ SGs, overexpression of *IRC* in *Ras*$^{V12}$ SGs also reduced SG size (Fig. S3F), improved tissue integrity and restored the SG lumen (Fig. 3R-V). In order to discriminate Idgf3 post- and transcriptional regulation, we performed qPCR on *IRC-OE;Ras*$^{V12}$ SGs and found a significantly lower level of *Idgf3* (Fig. 3K) in comparison to *Ras*$^{V12}$. The *Idgf3* reduction was only detectable in *IRC-OE;Ras*$^{V12}$ glands since ISH on SGS detected similar levels of Idgf3 transcripts in *CatA-OE;Ras*$^{V12}$ and *SodA-OE;Ras*$^{V12}$ in comparison to *Ras*$^{V12}$ SGs (Fig. 3G-J and S3G-L). Moreover, $H_2O_2$ affected JNK target gene expression, indicating a global regulation of JNK. This suggests that ROS, specifically $H_2O_2$, are involved in the activation of Idgf3 signaling and disruption of tissue integrity.

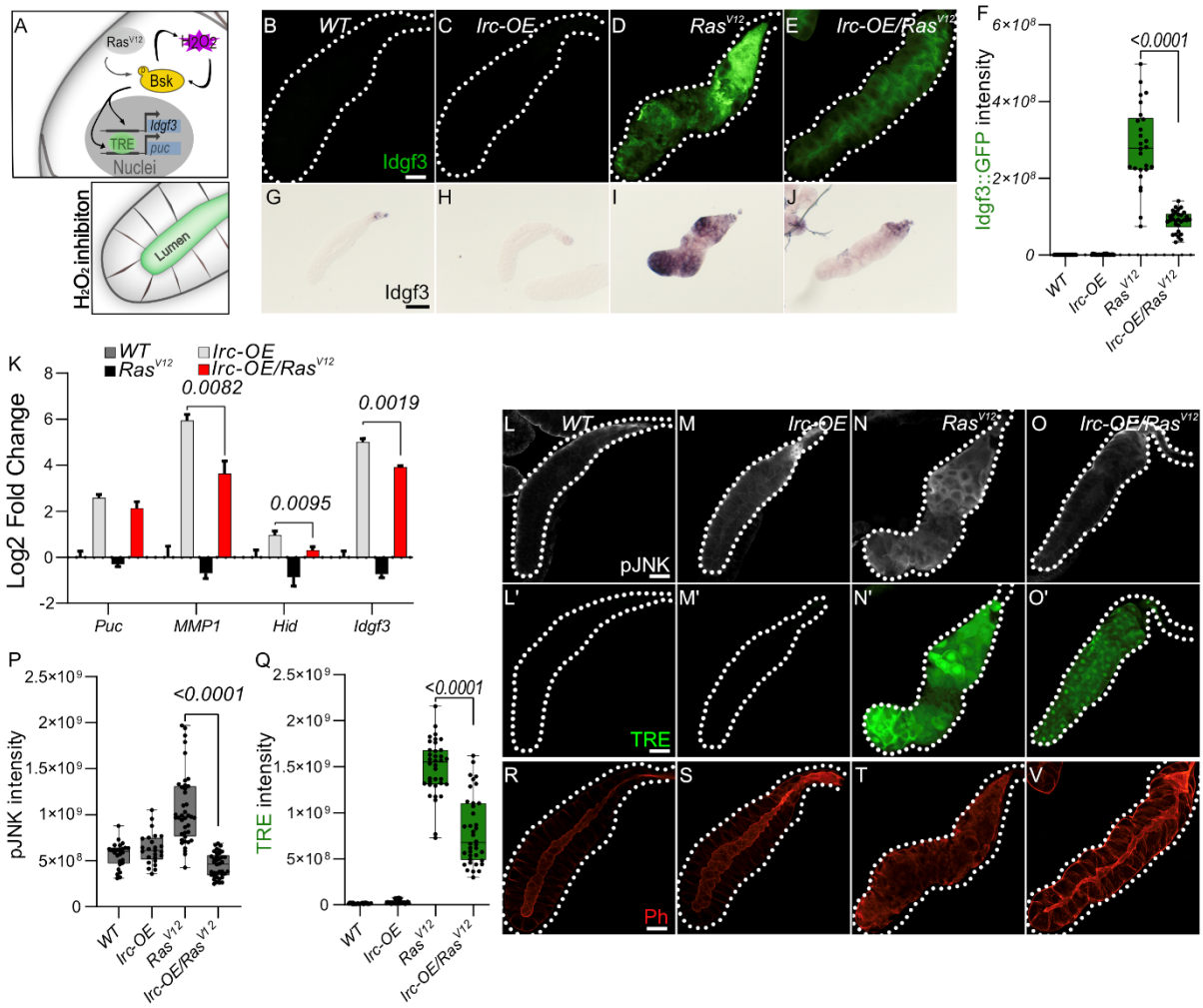


**Figure 3 *Idgf3* regulation feeds into a JNK-ROS feedback loop**
(A) $H_2O_2$, regulates *Idgf3* expression through JNK.
(B-E) Reduction of $H_2O_2$ by overexpression of secreted catalase (immune regulated catalase; IRC) lowered Idgf3::GFP levels (Quantified in F).
(G-J) ISH showing reduced expression of *Idgf3* in *IRC-OE;Ras$^{V12}$*glands.
(K) qPCR data showing reduction of *Idgf3, MMP1* and *Hid* in *IRC-OE;Ras$^{V12}$*glands.
(L-O') pJNK staining and TRE reporter constructs showing reduced intensity in *IRC-OE;Ras$^{V12}$* in comparison to *Ras$^{V12}$* glands, quantified in (P-Q).
(R-U) Phalloidin staining showing partially restored lumen in *IRC-OE;Ras$^{V12}$* glands.
Scale bars in (B-J, L-U) represent 100 $\mu$m. Data in (K) represent 3 independent replicas summarized as mean ± SD. Boxplot in (F,P-Q) represent at least 20 SG pairs. Whisker length min to max, bar represent median. P-value quantified with Student's t-test.

ROS mediates JNK activation through a positive feedback loop (Perez, Lindblad et al. 2017). Therefore we asked whether ROS induced *Idgf3* expression via the JNK-pathway. As done previously, we addressed pJNK and TRE.GFP levels. Interestingly, all tested ROS scavengers reduced pJNK levels (Fig. 3L-O, quantified in P, S3M-R, quantified in S) although TRE levels were not influenced in *SOD-OE;Ras$^{V12}$*, in contrast to *Cat-OE;Ras$^{V12}$* and *IRC-OE/Ras$^{V12}$* (Fig. 3L'-O', quantified in Q, S3M'-R', quantified in T). In summary, ROS contribute to the positive regulation of pJNK. In addition, overexpression of extracellular but not intracellular Catalase

reduces Idgf3 induction via JNK, indicating that *Idgf3* might be regulated via the secretory pathway. Duox and Nox, present in secretory glands, are transmembrane proteins that may generate extracellular ROS (Faria and Fortunato 2020). Their conserved function has been shown to facilitate tumor progression but whether they play an important role in $Ras^{V12}$ SGs remains to be elucidated (Aggarwal, Tuli et al. 2019).

**Idgf3 accumulates in enlarged vesicles**

We previously noted the uneven distribution of Idgf3 in $Ras^{V12}$ SGs (Fig. 1D). To further understand how Idgf3 promotes dysplasia, we dissected its subcellular localization in different areas of the SGs (Fig. 4A). We stained the glands for F-actin (Phalloidin) and addressed Idgf3::GFP localization at high resolution (Fig. 4B-C'). Interestingly, we observed Idgf3::GFP clusters surrounded by F-actin (Fig. 4C-C': arrow). Using a different salivary gland driver (*AB-Gal4*) to drive expression of $Ras^{V12}$, we also detected increased expression of Idgf3::GFP and localization within vesicle-like structures (Fig. S4A-B: arrow). The size of the vesicle-like structure was between 10-43 $\mu$m in comparison to secretory *Drosophila* vesicles (3-8$\mu$m, Fig. 4D, (Tran and Ten Hagen 2017)). We refer to these as enlarged vesicles (EnVs). Based on the increased Idgf3 levels, we wondered whether the protein was aggregating in EnVs.The aggregation marker, p62 (*Drosophila* Ref(2)P, (Bartlett, Isakson et al. 2011) detected signals throughout the cytoplasm of $Ras^{V12}$ *SGs*. In contrast, EnVs did not display any signs of aggregated proteins (Fig. S4C-D').

Since we had observed a loss of secretion in $Ras^{V12}$ *SGs* we next addressed the presence of EnVs within the secretory pathway. We overexpressed two versions of human phosphatidylserine binding protein, MFG-E8 (Milk fat globule-EGF factor), without (referred to as non-secreted: Fig .4F-F',I-I') and with a signal peptide (referred to as secreted: Fig. 4G-G',J-J', (Asano, Miwa et al. 2004)). In the controls, the non-secreted MFG-E8 was found in the cytoplasm, whereas the secreted version was detected in both the cytoplasm and in the lumen (Fig. 4F-G'). In $Ras^{V12}$ SGs, the non-secreted form was surrounding the EnVs (arrow), indicating the presence of phosphatidylserine on their membrane (Fig. 4I-I'). In contrast, the secreted form localized to the EnVs (Fig. 4J-J': arrow). These data suggest that (1) EnVs are surrounded by a lipid membrane and (2) EnVs likely derive from the secretory pathway.

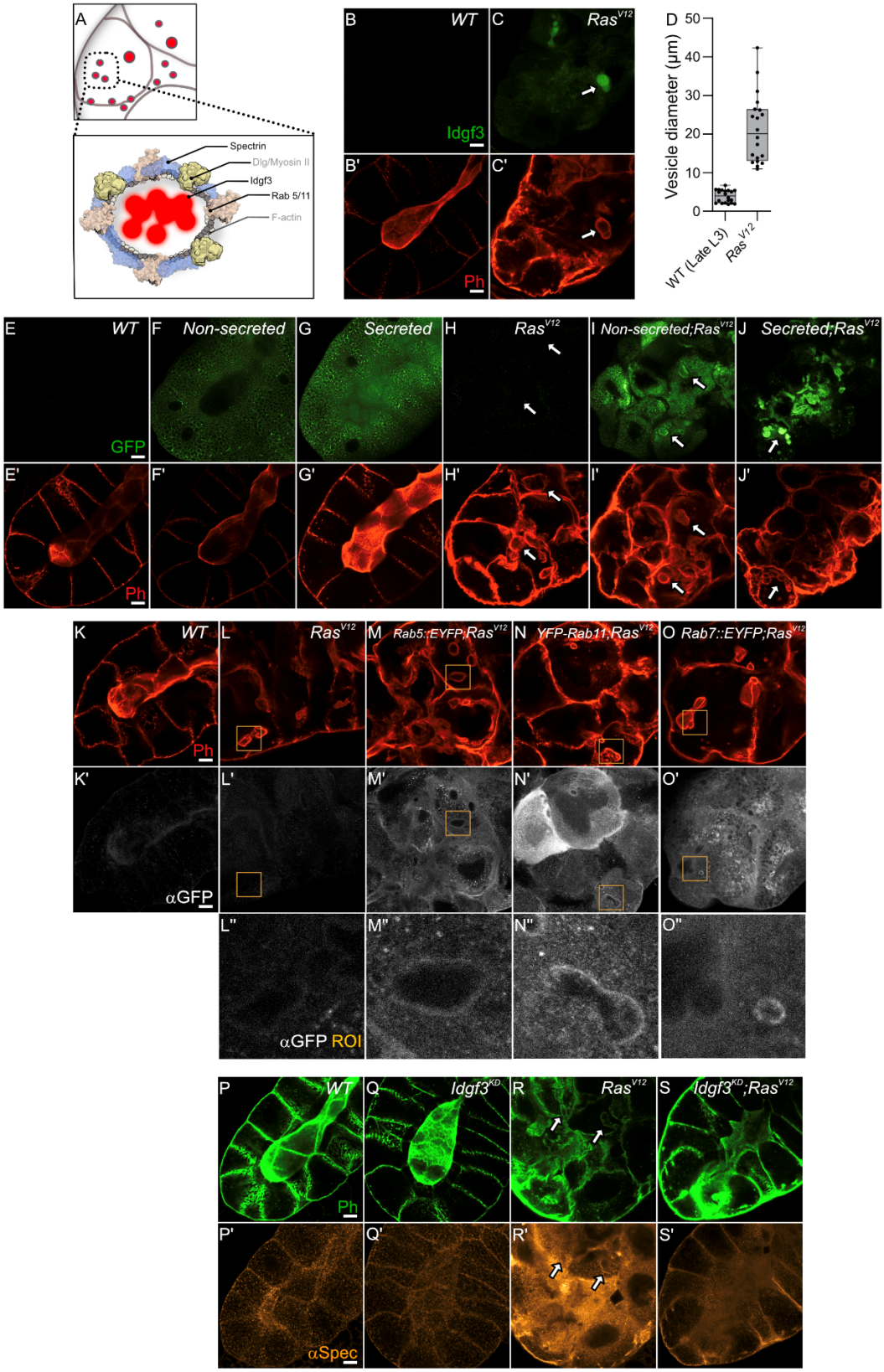


**Figure 4 *Idgf3* promotes formation of enlarged endosomes**

(A) Idgf3 enclosed by enlarged endosomes coated by cytoskeletal and cell polarity proteins.
(B-C') Idgf3::GFP clusters coated with Phalloidin.
(D) Vesicle size quantification showing *Ras*$^{V12}$ enlarged vesicles in comparison to prepupae SG vesicles.

(E-J') Non secreted MFGE8 localizes to the surface of EnVs, co-stained with phalloidin. The secreted MFGE8 is packaged into EnVs in *Ras*$^{V12}$glands.
(K-O'') Vesicle markers showing positively stained EnVs when detecting Rab5 and Rab11 but not Rab7.
(P-S') αSpectrin staining showing restoration of normal distribution in *Idgf3-KD;Ras*$^{V12}$glands. Scale bars in (B-C', E-J', K-O'' and P-S') represent 20 $\mu$m. Boxplot in (D) represent 20 EnVs. Whisker length min to max, bar represent median.

In order to further characterize Idgf3-positive EnVs we co-expressed vesicle-specific Rab's coupled with a GFP fluorophore, an autophagolysosomal marker (Atg8), an autophagy marker (Vps35), and a marker for phosphatidylinositol-3-phosphate-(PtdIns3P: *FYVE*)-containing endosomes in *Ras*$^{V12}$ glands (For a complete set see Fig. S4I-Q"). To increase sensitivity, we stained with anti-GFP and co-stained with Phalloidin. Localization of Rabs and phalloidin to the same vesicles was observed with Rab5 and Rab11 but not Rab7 (Fig. 4K-O'). Moreover, the EnVs were also positive for PtdIns3P (Fig. S4P-P"). In line with their dependence on secretion, this potentially identifies EnVs as enlarged recycling endosomes. EnV accumulation in *Ras*$^{V12}$ glands between 96 h and 120 h implies that (i) early endosome formation and fusion are either increased compared to *WT* or (ii) that recycling endosomes are not normally fused back to the apical membrane leading to their intracellular accumulation (Fig. S4E-H"). The latter hypothesis correlates with the loss of apico-basolateral polarity and the disruption of secretion due to a lack of a luminal structure ((Khalili, Kalcher et al. 2021) and Fig. S4E''-H"). To test the first hypothesis, we blocked the formation of early endosomes with *Rab5*$^{DN}$. Apico-basolateral polarity, detected by a visible lumen, was not affected by *Rab5*$^{DN}$. Moreover, *Rab5*$^{DN}$*;Ras*$^{V12}$ did not block EnV formation and restoration of apicobasal polarity (Fig. S4R-U: arrow). Halting the recycling endosome pathway via *Rab11*$^{DN}$ increased endosome accumulation without affecting cell polarity (Fig. S4V: arrow). In contrast, in *Rab11*$^{DN}$*;Ras*$^{V12}$ SGs, endosomes were not accumulating, and EnVs were still detected (Fig. S4W).Taken together, EnV formation is independent of the classical recycling pathway, suggesting other candidates are involved in the generation of EnVs.

**Idgf3 promotes loss of cell polarity via α-Spectrin positive enlarged endosomes**

Spectrins, cytoskeletal proteins which form a cortical network, have been shown to also play a role in secretion, cellular homeostas and cell polarity (Tjota, Lee et al. 2011, Lattner, Leng et al. 2019) all of which were affected in *Ras*$^{V12}$-SGs (Khalili, Kalcher et al. 2021). Therefore, we stained for αSpectrin, one of the three members of the spectrin family (Williams, Smith et al. 2003) and found it to localize to the EnVs (Fig. 4SX-Y'''). Moreover, we found markers for cell polarity including Dlg and Myosin II to also co-localize with the EnVs (Fig. S4Z—AC': arrow). Finally, we asked whether Idgf3 in *Ras*$^{V12}$ SGs was responsible for EnV formation and mislocalization of αSpectrin and found that indeed, *Idgf3-KD;Ras*$^{V12}$ glands lacked EnVs, and αSpectrin distribution was partially restored (Fig 4Q-T').

Taken together, Idgf3 promotes EnV formation and disruption of cellular integrity, assessed by mislocalization of αSpectrin, Dlg and Myosin II.

345 **Rac1 promotes the formation of EnVs via αSpectrin**

346 In SGs, overexpression of Rac generates enlarged vesicles coated with Spectrin (Lee and
347 Thomas 2011) with similarity to the EnVs described here. Therefore, we sought to investigate
348 the role of the Rac1 pathway in *Ras*$^{V12}$ glands (Fig. 5A). Supporting a role in dysplasia, *Ras*$^{V12}$
349 glands stained with Rac1 showed a stronger staining in comparison to the control. Moreover,
350 we observed Rac1 localized to EnVs (Fig. 5B-C'). To further assess Rac1's role in dysplasia
351 we overexpressed *Rac1*. Surprisingly, *Rac1-OE* alone was sufficient to induce *Idgf3*, an effect
352 that was not increased in *Rac1-OE*;*Ras*$^{V12}$ (Fig. 5D-E, I-J). Due to the pleiotropic effects of the
353 *Rac1*$^{DN}$ construct, we addressed Rac1 function by modulating the expression of the Rac1
354 effector molecule, *Pak* (Lee and Thomas 2011). *Pak-KD*;*Ras*$^{V12}$ did not reduce *Idgf3* levels but
355 improved the histology of the gland (Fig. 5I,K). Conversely, overexpression of *Pak*$^{CA}$ did not
356 increase *Idgf3* levels and had no detectable effect on F-actin distribution (Fig S5A-C''). In
357 contrast, Rac1 activity via Pak does affect *Ras*$^{V12}$ SG integrity: Idgf3::GFP levels were increased
358 in *Rac1-OE* SGs and F-actin was disorganized (Fig. S5D-F'', quantified in I). However, the
359 *Rac1-OE* glands did not grow larger compared to *Ras*$^{V12}$, indicating additional signals are
360 necessary for gland overgrowth. Also, *Pak-KD*;*Ras*$^{V12}$ SGs displayed a more regular F-actin
361 distribution leading to restoration of the lumen and proper secretion of Idgf3 (Fig. S5G-H'').

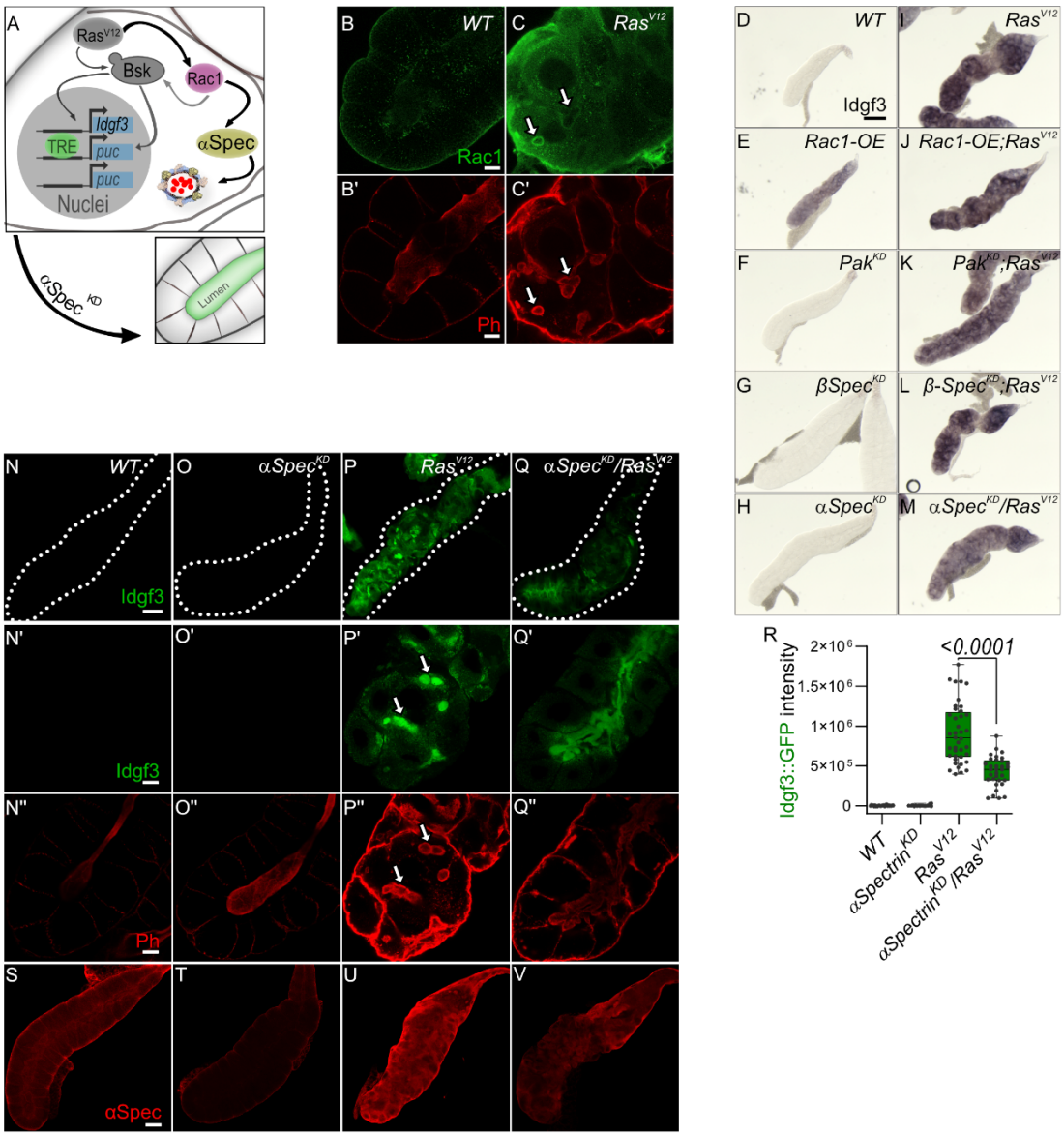


**Figure 5 Rac1 promotes EnVs formation through αSpectrin?**
(A) Redistribution of the spectrin-based membrane skeleton (SBMS) facilitates loss of cell polarity through Idgf3 packed EnVs.
(B-C') Rac1 staining showing EnVs co-localizing with Phalloidin.
(D-M) ISH showing increased *Idgf3* staining in *Rac1-OE* glands. Improved tissue structure in *Pak-KD;Ras$^{V12}$* and *αSpectrin*-KD/*Ras$^{V12}$* glands did not affect *Idgf3* expression in comparison to *Ras$^{V12}$*.
(N-V) Reduced levels of αSpectrin (αSpectrin-*KD* /*Ras$^{V12}$*) reduces Idgf3::GFP levels quantified in (R) prevents formation of EnVs and largely restores the SG lumen (arrows indicate EnVs). αSpectrin staining (S-V) is quantified in (S5V).
Scale bars in (B-C' and N'-Q'') represent 20 $\mu$m, (D-M) 0.3 mm and (N-Q and S-V) 100 $\mu$m. Boxplot in (R) represent at least 20 SG pairs. Whisker length min to max, bar represent median. P-value quantified with Student's t-test.

To further characterize the Rac1 pathway, we asked whether the downstream components *β-Spec* and *αSpec* affected *Idgf3* transcript levels in *Ras$^{V12}$* glands. I*dgf3*-specific ISH of *β-Spec-KD;Ras$^{V12}$* or *αSpec-KD/Ras$^{V12}$* showed that this was not the case. However, SG histology

380 improved in *αSpec-KD/Ras*$^{V12}$ (Fig 5I, L-M). Therefore, we further looked into *αSpec-*
381 *KD/Ras*$^{V12}$ and its effect on F-actin organization and noted a similar effect as in *Pak-KD;Ras*$^{V12}$
382 (Fig 5N-Q'), namely that Idgf3::GFP levels were reduced. However, most of the Idgf3::GFP
383 signal was detectable in the lumen (Fig. 5Q-Q', quantified in R). The ISH was substantiated
384 with qPCR which showed increased levels of *Idgf3* in *Rac1-OE*, slightly increased levels in
385 *Pak*$^{CA}$, whereas *αSpec-KD/Ras*$^{V12}$ showed a slight reduction (Fig. S5J). Moreover, JNK target
386 genes, such as *Puc* and *Grnd* were upregulated in *Rac1-OE* and to some extent in *Pak*$^{CA}$ (Fig.
387 S5J). Supporting regulation of JNK target genes via JNK, *Rac1-OE* showed higher TRE level
388 compared to *Pak*$^{CA}$ (Fig. S5K-M'', quantified in N and O). Interestingly, *αSpec-KD/Ras*$^{V12}$
389 reduced JNK and TRE levels (Fig S5P-S, quantified in T and U) without affecting JNK target
390 genes (Fig. S5J). In summary, *Rac1-OE* was sufficient to induce *Idgf3* in salivary glands.
391 However, in *Ras*$^{V12}$ SGs, additional signals contribute to *Idgf3* regulation. This is most likely
392 due to additional effectors feeding into JNK signaling. Our data suggest, downregulation and
393 upregulation of the JNK pathway may have different outcomes at the transcriptional and post-
394 transcriptional level. Nevertheless, αSpectrin promotes EnV formation in *Ras*$^{V12}$ SGs, disrupts
395 polarity, proper secretion, and localization of Idgf3.

396 **JNK promotes EnV formation via Idgf3 upstream of αSpectrin**

397 The data presented here suggest that Idgf3 promotes EnV formation (Fig. 4R-S). Moreover,
398 this likely occurs post-transcriptionally (Fig. S6A) since *Idgf3-KD;Ras*$^{V12}$ did not lead to
399 reduced expression of *aSpectrin*. In contrast, at 96 hours, overexpression of Idgf3 throughout
400 the whole gland, as shown by ISH (Fig. S6B-E), led to an increase in the number of glands with
401 endosomes (Fig. S6F-I''', quantified in J). The observed activation of αSpec via Idgf3
402 prompted us to investigate the epistasis between JNK, Idgf3, Rac1, and αSpec. First, we
403 addressed epistasis between Idgf3 and JNK since blocking JNK function by expressing a
404 dominant-negative form (*Bsk*$^{DN}$) resulted in restoration of apical-basal polarity (Fig. S6F-G).
405 We calculated the penetrance of EnVs formation when we blocked JNK and overexpressed
406 *Idgf3* (*Idgf3-OE*). In *Ras*$^{V12}$ SGs we observed EnVs in 100 % of the glands, an effect that was
407 strongly blocked in *JNK*$^{DN}$*;;Ras*$^{V12}$ (Fig. 6 F-G, quantified in K). Blocking JNK and
408 overexpressing *Idgf3* in *Ras*$^{V12}$ strongly reverted the *JNK*$^{DN}$*;;Ras*$^{V12}$ phenotype - a lumen could
409 not be detected, and around 98% of the glands contained enlarged endosomes (Fig. 6F,I,
410 quantified in K). Overexpression of Idgf3 alone did not result in EnV formation (Fig. 6B-E). In
411 conclusion, the data suggest that Idgf3 acts downstream of JNK and through formation of EnV's
412 which disrupts luminal integrity.

413 αSpectrin has been shown to act downstream of Rac1 (Lee and Thomas 2011). With our *Bx*
414 driver, we could reproduce this epistasis. *Rac1-OE* was sufficient to interfere with apicobasal
415 polarity without forming detectable EnVs, and this phenotype was reverted in *Rac1-OE;αSpec-*
416 *KD* (Fig. S6K-O). In order to find out whether the same epistasis takes place between Rac1 and
417 αSpectrin in *Ras*$^{V12}$ glands, we investigated luminal integrity. In *Rac1-OE;αSpec-KD/Ras*$^{V12}$,
418 partial restoration of the lumen was observed, indicating that apicobasal polarity improved (Fig.
419 S6 L, P-Q). Moreover, *Pak-KD;Ras*$^{V12}$ showed lower αSpectrin levels in comparison to *Ras*$^{V12}$
420 (Fig. S6S,W quantified in Y). This suggests that αSpectrin acts downstream of Rac1 in *Ras*$^{V12}$
421 glands.

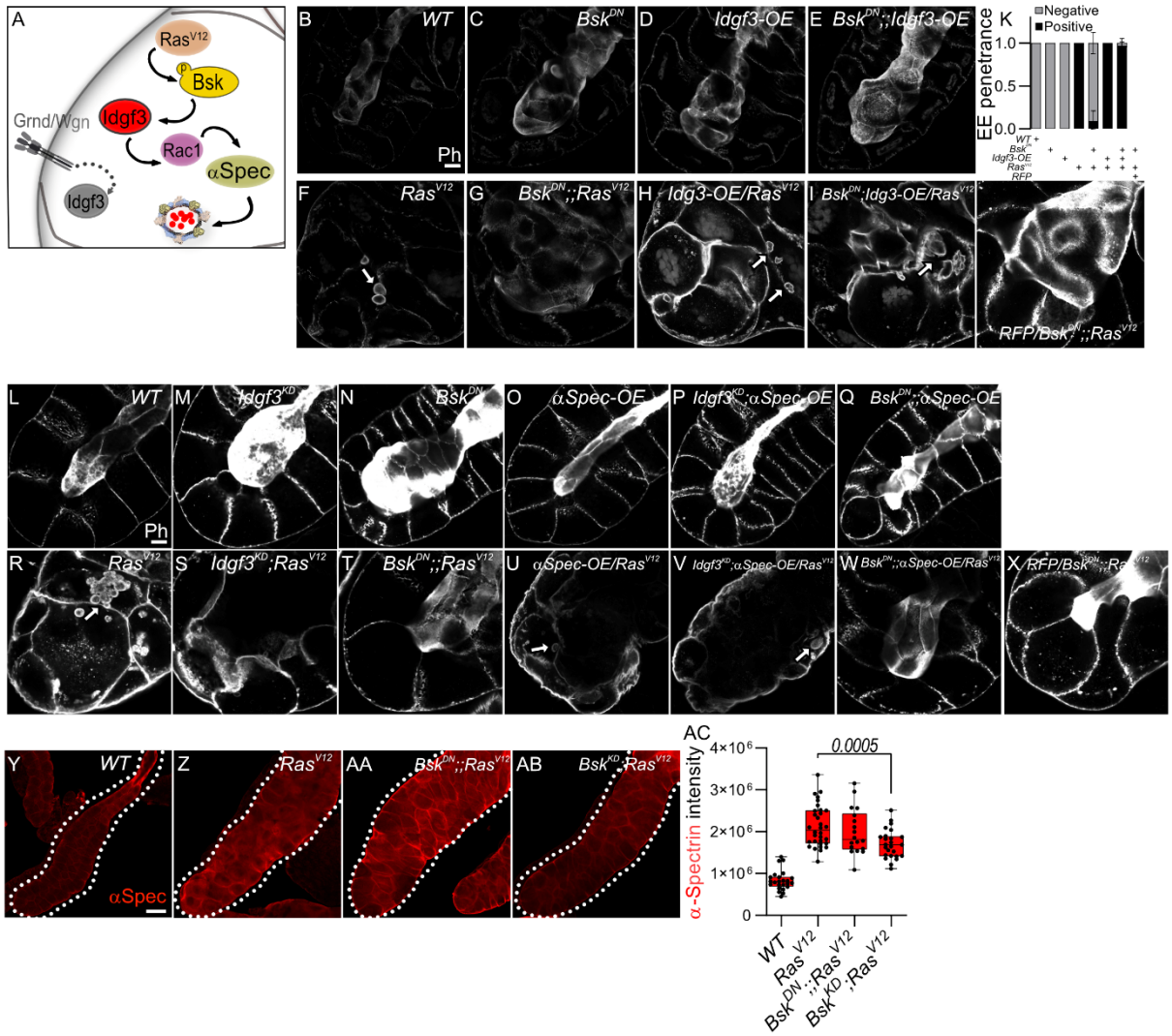


**Figure 6 Idgf3 promotes activation of Rac1 and loss of cell polarity through αSpectrin**
(A) Idgf3 promotes formation of EnVs, upstream of Rac1.
(B-J) Phalloidin staining showing epistasis of EnVs formation in which Idgf3 acts downstream of JNK.
(K) EnVs penetrance quantification showing a strong induction of EnVs in *JNK$^{DN}$;;Idgf3-OE/Ras$^{V12}$* glands.
(L-X) Epistatic analysis between Idgf3 and αSpectrin. Phalloidin staining showing EnVs presence in *Idgf3-KD;αSpec-OE/ Ras$^{V12}$*.
(Y-AB) αSpectrin levels were reduced in *JNK-KD;Ras$^{V12}$* in comparison to *Ras$^{V12}$* but not in *JNK$^{DN}$;Ras$^{V12}$* glands, quantified in (AC).
Scale bars in (B-J and L-X) represent 20 $\mu$m and (Y-AB) 100 $\mu$m. Barplot in (K) represent 3 independent replicas with at least 10 SG pairs, summarized a mean ± SD. Boxplot in (AC) represent at least 19 SG pairs. Whisker length min to max, bar represent median. P-value quantified with Student's t-test.

To further dissect the epistasis between JNK-Idgf3 and Rac1-αSpectrin in *Ras$^{V12}$* glands, we addressed the relationship between Idgf3 and αSpectrin by addressing luminal integrity. As previously described, *Idgf3-KD;Ras$^{V12}$* SGs showed a partially restored lumen, an indication of an improved apicobasal polarity (Fig. 6R-S).Moreover, the glands displayed lower αSpectrin

442 levels in comparison to *Ras*$^{V12}$ (Fig.4R-S). Conversely, *Idgf3-KD;αSpec-OE/ Ras*$^{V12}$ glands
443 displayed weak F-actin staining and rounded cells containing EnVs (Fig. 6R,V). This suggests
444 that αSpec acts downstream of Idgf3. In contrast, *JNK*$^{DN}$*;;αSpec-OE/ Ras*$^{V12}$ SGs did not lose
445 their polarity shown by F-actin staining, indicating that αSpec acts upstream of JNK, a
446 phenotype independent of the dilution of the driver (Fig. 6R,W-X).

447 The unexpected epistatic relationship between Idgf3 and αSpectrin downstream of JNK (Fig.
448 6L-X) led us to speculate whether the levels of JNK might play a role. Indeed, staining the
449 gland for αSpectrin showed no significant difference in the intensity between *Ras*$^{V12}$ and
450 *JNK*$^{DN}$*;;Ras*$^{V12}$ (Fig. S6R-V, quantified in W). Conversely, when we used *JNK-KD* to diminish
451 JNK levels, the levels of αSpectrin were also reduced (in *JNK-KD;Ras*$^{V12}$*)* when compared to
452 *Ras*$^{V12}$ alone (Fig. 6Y-AB, quantified in AC). These data indicate a complex interaction between
453 JNK levels and disruption of apicobasal polarity mediated by Idgf3 via αSpectrin. In summary,
454 Idgf3 promotes endosome formation via increased levels of αSpec, and as a result, the SGs lose
455 apicobasal polarity and overgrow.

456

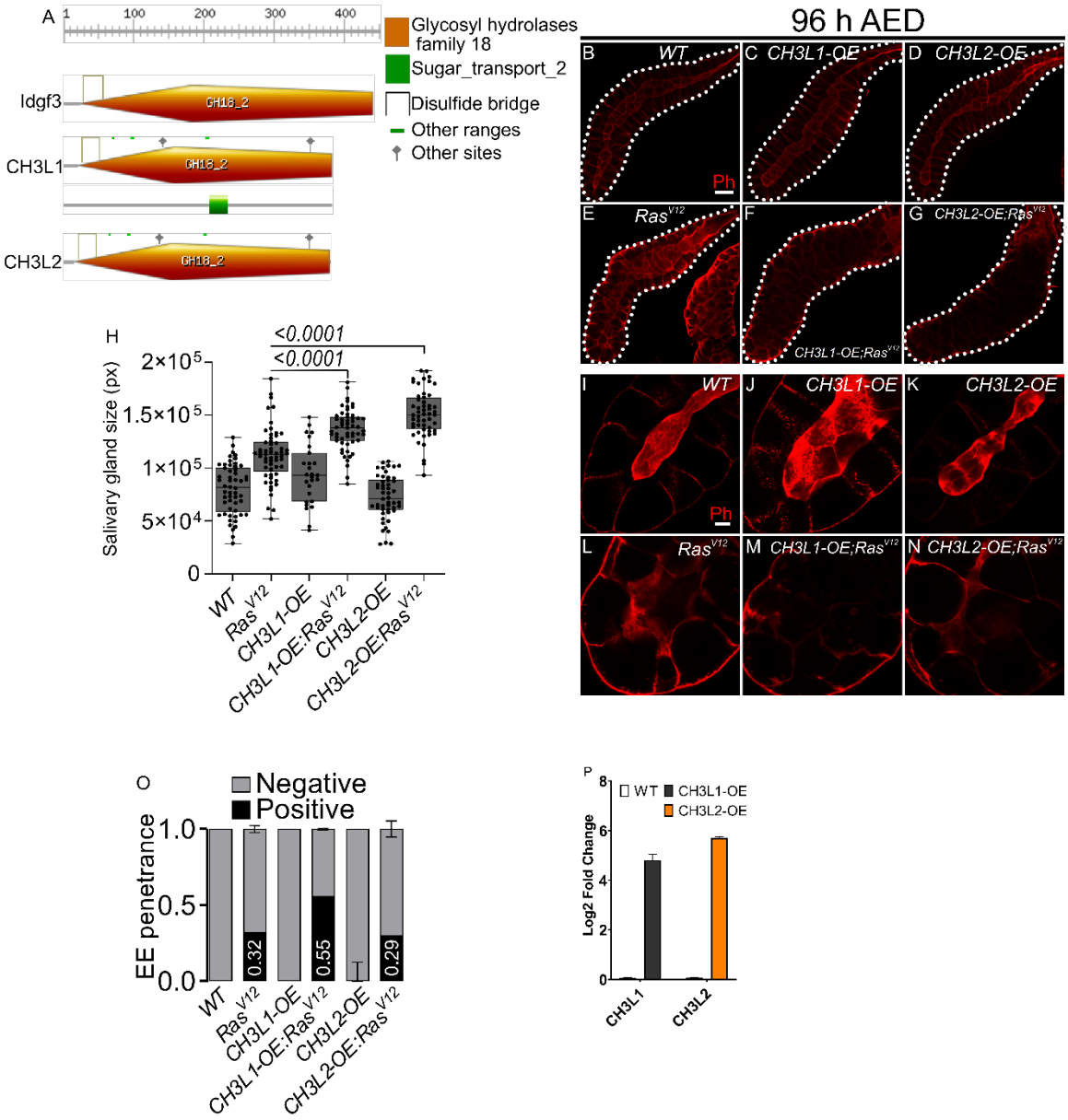


**Figure 7 Human Chitinase-like proteins similarly to Idgf3 promotes EnVs formation**

(A) Comparison of Idgf3, CH3L1 and CH3L2 protein motifs (https://prosite.expasy.org).
(B-G) Representative images of phalloidin staining used for size quantification.
(H) SG size quantification showing an increase in tissue size in *CH3L1-OE;Ras*$^{V12}$ and *CH3L2-OE;Ras*$^{V12}$ SG compared to *Ras*$^{V12}$ alone.
(I-N) Phalloidin staining depicting disrupted lumen integrity in *Ras*$^{V12}$ glands.
(O) EnVs penetrance quantification showing an induction of EnVs in *CH3L1-OE;Ras*$^{V12}$ glands.
(P) qPCR confirmation of CH3L1 and CH3L2 expression in SG.
Scale bars in (B-G) represent 100 $\mu$m and (I-N) 20 $\mu$m. Boxplot in (H) represent at least 19 SG pairs. Whisker length min to max, bar represent median. P-value quantified with Student's t-test. Barplot in (O) represent 3 independent replicas with at least 10 SG pairs, summarized as

470 mean ± SD. Column chart in (P) represent 4 independent replicas with at least 10 SG pairs,
471 summarized as mean ± SD.
472
473 **Human CLP members enhance dysplasia in *Drosophila* SGs.**

474 Finally, we also wished to determine whether the tumor-modulating effects we had observed
475 for *Drosophila* Idgf3 also applied to human CLP members. For this we expressed two human
476 *CLPs* (*Ch3L1* or *Ykl-40*; 29% AA identity and *Ch3L2* or *Ykl-39*; 26% AA identity, Fig. 7A) in
477 SGs, both on their own and in combination with $Ras^{V12}$. Similar to Idgf3, both CLPs enhanced
478 the hypertrophy observed in $Ras^{V12}$ SGs (Fig. 7 B-K and O). Additionally, *Ch3L1* enhanced the
479 prevalence of EnVs in the Ras mutant background. Taken together this means that the tumor-
480 promoting effect of CLPs is conserved between *Drosophila* and humans and may affect
481 different phenotypes of dysplasia depending on the CLP under study.

482

483 **Discussion**

484 The levels of Chitinase-like proteins (CLPs) are elevated during a wide range of inflammatory
485 regenerative and neoplastic disorders. Their physiological function has been more elusive but
486 includes regenerative processes such as the restoration of cell integrity after oxidative damage
487 (Lee, Da Silva et al. 2011). Induction of CLPs has been associated with cancer development
488 with poor prognosis (reviewed in (Zhao, Su et al. 2020)), but their role in ductal tumors is
489 understudied. We used *Drosophila* as a tumor model to dissect CLP (*Idgf3*) function genetically
490 in a highly secretory ductal organ, the salivary glands. We show that Idgf3 promotes tumor
491 overgrowth through the disruption of cell polarity. The tissue and cell-autonomous induction
492 of *Idgf3* disrupts cell organization and leads to the formation of enlarged endosome vesicles
493 (EnVs) that accumulate in the cytoplasm. Genetically, *Idgf3* is induced via a pro-tumorigenic
494 JNK and ROS signaling feedback loop. Consequently, Idgf3 disrupts the organization of the
495 spectrin-based membrane skeleton (SBMS) through formation of EnVs via activation of Rac1.
496 Significantly, KD of *Idgf3* inhibits overgrowth, restores cell polarity, and reduces ECM size
497 and nuclear volume through blockage of EnV formation.

498 Our identification of a contribution of JNK sigaling and both extra- and intracellular ROS to
499 dysplasia is in line with previous findings from other *Drosophila* tumor models (Fogarty and
500 Bergmann 2017). Similarly, we observe an amplification loop between ROS and JNK signaling,
501 which augments the dysplastic phenotype ((Krautz, Khalili et al. 2020)). Several studies have
502 demonstrated that activation of JNK signaling in mammals promotes the progression of ductal
503 tumors (Yeh, Hou et al. 2006, Tang, Sun et al. 2013, Insua-Rodriguez, Pein et al. 2018). Here
504 we identify Idgf3 as an additional component that feeds into JNK signaling, possibly in a
505 concentration dependent manner (Fig. 6). Ultimately in $Ras^{V12}$-expressing SGs, this leads to the
506 formation of EnVs involving Spectrins. Members of the Spectrin family have a supporting role
507 in providing cellular architecture through interaction with phospholipids and actively
508 promoting polymerization of F-actin (Juliano, Kimelberg et al. 1971, Pinder, Bray et al. 1975,
509 Hardy and Schrier 1978). Moreover, the secretory activity of ductal organs has been shown to
510 be facilitated by Spectrins (Lattner, Leng et al. 2019).

511 During *Drosophila* development and under physiological conditions, the pathway that involves
512 Spectrins, Rac1 and Pak1 has been shown to be required for the maintenance of cell polarity
513 while when deregulated, it leads to the formation of enlarged vesicles similar to the EnVs(Lee
514 and Thomas 2011). Thus our results provide a possible link between the observed induction of
515 CLPs in a range of tumors and the effects of Spectrins and their deregulation (Ackermann and
516 Brieger 2019, Yang, Yang et al. 2021). In addition to the genetic interaction, previous work
517 suggests a mechanical link between spectrins via a Spectrin binding protein Hssh3bp1 (Human
518 spectrin Src homology domain binding protein1; (Ziemnicka-Kotula, Xu et al. 1998)), the loss
519 of which has been associated with prostatic tumors (Macoska, Xu et al. 2001). Hhh3bp1 may
520 influence tumor progression possibly through interaction with tyrosine kinases such as Abelson
521 tyrosine kinase (Macoska, Xu et al. 2001). Interestingly Hhh3bp1 is a marker and possible
522 regulator of macropinocytosis, a recycling pathway that is known to be hijacked by Ras-
523 transformed tumor cells to acquire nutrients (Recouvreux and Commisso 2017) and also leads
524 to the formation of large intracellular vesicles. In favour of this hypothesis, macropinocytosis
525 has been found to depend on Rac1/Pak1 signaling, although the resulting vesicles are usually
526 smaller (0.2-5 micrometers) than EnVs (Maxson, Sarantis et al. 2021). We find that - like
527 macropinocytosis - EnV-formation depends on the activity of growth factor receptors
528 (Recouvreux and Commisso 2017), in this case Idgf3, much in line with its original description
529 as an *in vitro* mediator of insulin signaling (Kawamura, Shibata et al. 1999). *In vivo*, under
530 normal conditions, Idgf3 is required for proper formation of chitin-containing structures, wound
531 healing and cellular integrity (Pesch, Riedel et al. 2016). Thus, under these circumstances Idgf3
532 may help to preserve SG integrity including the epithelial character of SG cells upstream of
533 spectrins. Conversely, in a non-physiological setting such as upon overexpression of $Ras^{V12}$,
534 this mechanism is overwhelmed leading to the breakdown of homeostasis, loss of cell polarity
535 and the gland lumen, loss of secretory activivity and the formation of EnVs larger than
536 macropinocytic vesicles. In a mammalian setting, the associated phenotypes such as disruption
537 of cellular polarity and reorganization of the ECM provide targets for therapeutic treatments
538 (Insua-Rodriguez, Pein et al. 2018). Depending on the tissue environment, CLP's may have
539 various roles in a context-dependent manner. Overexpression of *Idgf3* alone is not sufficient for
540 the loss of cell polarity, growth, and fibrosis. Collectively, this suggests a tumor-specific
541 phenotype for Idgf3 (Fig. 6B-J), similar to mammalian CLPs (reviewed in (Zhao, Su et al.
542 2020)). In support for a phylogenetically conserved contribution of CLPs to tumor progression,
543 we were able to recapitulate SG hypertrophy and EnV formation when we expressed two human
544 CLPs in $Ras^{V12}$ SGs. Whether the differences we observe between the two human CLPs is due
545 to their different structure awaits further work. Similarly, due to their pleiotropic effects, further
546 investigation of the role of CLPs will be required to dissect their molecular function in a given
547 tissue and to ultimately design tumor-specific treatments (Kzhyshkowska, Larionova et al.
548 2019).

549 Taken together our findings provide new insight into the loss of tissue integrity in a neoplastic
550 tumor model and provide targets to test how developmentally and physiologically important
551 deregulated mechanisms contribute to tumor progession in certain forms of cancer.

552

553 **Acknowledgments**

554 We would like to thank Chris Molenaar, Roger Karlsson, Stina Höglund and the Imaging
555 facility at Stockholm University for support with all aspects of microscopy. We would also
556 like to thank Vasilios Tsarouhas for his critical feedback. This work was supported by grants
557 from the Swedish Cancer Foundation (CAN 2015-546), the Wenner-Gren Foundation
558 (UPD2020-0094 and UPD2021-0095 to MK) and the Swedish Research Council (VR 2016-
559 04077 and VR 2021-04841).

560

561 **References**

562

563 Ackermann, A. and A. Brieger (2019). "The Role of Nonerythroid Spectrin alphaII in Cancer."
564 J Oncol **2019**: 7079604.
565 Aggarwal, V., H. S. Tuli, A. Varol, F. Thakral, M. B. Yerer, K. Sak, M. Varol, A. Jain, M. A.
566 Khan and G. Sethi (2019). "Role of Reactive Oxygen Species in Cancer Progression:
567 Molecular Mechanisms and Recent Advancements." Biomolecules **9**(11).
568 Andersen, D. S., J. Colombani, V. Palmerini, K. Chakrabandhu, E. Boone, M. Rothlisberger, J.
569 Toggweiler, K. Basler, M. Mapelli, A. O. Hueber and P. Leopold (2015). "The Drosophila
570 TNF receptor Grindelwald couples loss of cell polarity and neoplastic growth." Nature
571 **522**(7557): 482-486.
572 Archibald, A., C. Mihai, I. G. Macara and L. McCaffrey (2015). "Oncogenic suppression of
573 apoptosis uncovers a Rac1/JNK proliferation pathway activated by loss of Par3." Oncogene
574 **34**(24): 3199-3206.
575 Asano, K., M. Miwa, K. Miwa, R. Hanayama, H. Nagase, S. Nagata and M. Tanaka (2004).
576 "Masking of phosphatidylserine inhibits apoptotic cell engulfment and induces autoantibody
577 production in mice." J Exp Med **200**(4): 459-467.
578 Baek, S. H., Y. C. Kwon, H. Lee and K. M. Choe (2010). "Rho-family small GTPases are
579 required for cell polarization and directional sensing in Drosophila wound healing."
580 Biochem Biophys Res Commun **394**(3): 488-492.
581 Bartlett, B. J., P. Isakson, J. Lewerenz, H. Sanchez, R. W. Kotzebue, R. C. Cumming, G. L.
582 Harris, I. P. Nezis, D. R. Schubert, A. Simonsen and K. D. Finley (2011). "p62, Ref(2)P and
583 ubiquitinated proteins are conserved markers of neuronal aging, aggregate formation and
584 progressive autophagic defects." Autophagy **7**(6): 572-583.
585 Bennett, V. and A. J. Baines (2001). "Spectrin and ankyrin-based pathways: metazoan
586 inventions for integrating cells into tissues." Physiol Rev **81**(3): 1353-1392.
587 Brumby, A. M. and H. E. Richardson (2003). "scribble mutants cooperate with oncogenic Ras
588 or Notch to cause neoplastic overgrowth in Drosophila." EMBO J **22**(21): 5769-5779.
589 Ciapponi, L., D. B. Jackson, M. Mlodzik and D. Bohmann (2001). "Drosophila Fos mediates
590 ERK and JNK signals via distinct phosphorylation sites." Genes Dev **15**(12): 1540-1553.
591 Diwanji, N. and A. Bergmann (2017). "The beneficial role of extracellular reactive oxygen
592 species in apoptosis-induced compensatory proliferation." Fly (Austin) **11**(1): 46-52.
593 Faria, C. C. and R. S. Fortunato (2020). "The role of dual oxidases in physiology and cancer."
594 Genet Mol Biol **43**(1 suppl. 1): e20190096.
595 Fernandez-Medarde, A., J. De Las Rivas and E. Santos (2021). "40 Years of RAS-A Historic
596 Overview." Genes (Basel) **12**(5).

597 Fletcher, G. C., A. Elbediwy, I. Khanal, P. S. Ribeiro, N. Tapon and B. J. Thompson (2015).
598 "The Spectrin cytoskeleton regulates the Hippo signalling pathway." EMBO J **34**(7): 940-
599 954.
600 Fogarty, C. E. and A. Bergmann (2017). "Killers creating new life: caspases drive apoptosis-
601 induced proliferation in tissue repair and disease." Cell Death Differ **24**(8): 1390-1400.
602 Hardy, B. and S. L. Schrier (1978). "The role of spectrin in erythrocyte ghost endocytosis."
603 Biochem Biophys Res Commun **81**(4): 1153-1161.
604 Igaki, T., R. A. Pagliarini and T. Xu (2006). "Loss of cell polarity drives tumor growth and
605 invasion through JNK activation in Drosophila." Curr Biol **16**(11): 1139-1146.
606 Insua-Rodriguez, J., M. Pein, T. Hongu, J. Meier, A. Descot, C. M. Lowy, E. De Braekeleer,
607 H. P. Sinn, S. Spaich, M. Sutterlin, A. Schneeweiss and T. Oskarsson (2018). "Stress
608 signaling in breast cancer cells induces matrix components that promote chemoresistant
609 metastasis." EMBO Mol Med **10**(10).
610 Johansen, J. S., B. V. Jensen, A. Roslind, D. Nielsen and P. A. Price (2006). "Serum YKL-40,
611 a new prognostic biomarker in cancer patients?" Cancer Epidemiol Biomarkers Prev **15**(2):
612 194-202.
613 Juliano, R. L., H. K. Kimelberg and D. Papahadjopoulos (1971). "Synergistic effects of a
614 membrane protein (spectrin) and Ca 2+ on the Na + permeability of phospholipid vesicles."
615 Biochim Biophys Acta **241**(3): 894-905.
616 Kanda, H., T. Igaki, H. Kanuka, T. Yagi and M. Miura (2002). "Wengen, a member of the
617 Drosophila tumor necrosis factor receptor superfamily, is required for Eiger signaling." J
618 Biol Chem **277**(32): 28372-28375.
619 Karlsson, C., A. M. Korayem, C. Scherfer, O. Loseva, M. S. Dushay and U. Theopold (2004).
620 "Proteomic analysis of the Drosophila larval hemolymph clot." J Biol Chem **279**(50): 52033-
621 52041.
622 Kawamura, K., T. Shibata, O. Saget, D. Peel and P. J. Bryant (1999). "A new family of growth
623 factors produced by the fat body and active on Drosophila imaginal disc cells." Development
624 **126**(2): 211-219.
625 Khalili, D., C. Kalcher, S. Baumgartner and U. Theopold (2021). "Anti-Fibrotic Activity of an
626 Antimicrobial Peptide in a Drosophila Model." J Innate Immun: 1-15.
627 Khalili, D., C. Kalcher, S. Baumgartner and U. Theopold (2021). "Anti-Fibrotic Activity of an
628 Antimicrobial Peptide in a Drosophila Model." J Innate Immun **13**(6): 376-390.
629 Kirkpatrick, R. B., R. E. Matico, D. E. McNulty, J. E. Strickler and M. Rosenberg (1995). "An
630 abundantly secreted glycoprotein from Drosophila melanogaster is related to mammalian
631 secretory proteins produced in rheumatoid tissues and by activated macrophages." Gene
632 **153**(2): 147-154.
633 Krautz, R., D. Khalili and U. Theopold (2020). "Tissue-autonomous immune response regulates
634 stress signalling during hypertrophy." Elife **9**.
635 Kucerova, L., O. I. Kubrak, J. M. Bengtsson, H. Strnad, S. Nylin, U. Theopold and D. R. Nassel
636 (2016). "Slowed aging during reproductive dormancy is reflected in genome-wide
637 transcriptome changes in Drosophila melanogaster." BMC Genomics **17**(1): 50.
638 Kzhyshkowska, J., I. Larionova and T. Liu (2019). "YKL-39 as a Potential New Target for
639 Anti-Angiogenic Therapy in Cancer." Front Immunol **10**: 2930.
640 Lattner, J., W. Leng, E. Knust, M. Brankatschk and D. Flores-Benitez (2019). "Crumbs
641 organizes the transport machinery by regulating apical levels of PI(4,5)P2 in Drosophila."
642 Elife **8**.
643 Lee, C. G., C. A. Da Silva, C. S. Dela Cruz, F. Ahangari, B. Ma, M. J. Kang, C. H. He, S.
644 Takyar and J. A. Elias (2011). "Role of chitin and chitinase/chitinase-like proteins in
645 inflammation, tissue remodeling, and injury." Annual review of physiology **73**: 479-501.

646 Lee, S. K. and G. H. Thomas (2011). "Rac1 modulation of the apical domain is negatively
647 regulated by beta (Heavy)-spectrin." Mech Dev **128**(1-2): 116-128.
648 Macoska, J. A., J. Xu, D. Ziemnicka, T. S. Schwab, M. A. Rubin and L. Kotula (2001). "Loss
649 of expression of human spectrin src homology domain binding protein 1 is associated with
650 10p loss in human prostatic adenocarcinoma." Neoplasia **3**(2): 99-104.
651 Maxson, M. E., H. Sarantis, A. Volchuk, J. H. Brumell and S. Grinstein (2021). "Rab5 regulates
652 macropinocytosis by recruiting the inositol 5-phosphatases OCRL and Inpp5b that hydrolyse
653 PtdIns(4,5)P2." J Cell Sci **134**(7).
654 Morera, E., S. S. Steinhauser, Z. Budkova, S. Ingthorsson, J. Kricker, A. Krueger, G. A.
655 Traustadottir and T. Gudjonsson (2019). "YKL-40/CHI3L1 facilitates migration and
656 invasion in HER2 overexpressing breast epithelial progenitor cells and generates a niche for
657 capillary-like network formation." In Vitro Cell Dev Biol Anim **55**(10): 838-853.
658 Pagliarini, R. A. and T. Xu (2003). "A genetic screen in Drosophila for metastatic behavior."
659 Science **302**(5648): 1227-1231.
660 Palmerini, V., S. Monzani, Q. Laurichesse, R. Loudhaief, S. Mari, V. Cecatiello, V. Olieric, S.
661 Pasqualato, J. Colombani, D. S. Andersen and M. Mapelli (2021). "Drosophila TNFRs
662 Grindelwald and Wengen bind Eiger with different affinities and promote distinct cellular
663 functions." Nat Commun **12**(1): 2070.
664 Park, K. R., H. M. Yun, K. Yoo, Y. W. Ham, S. B. Han and J. T. Hong (2020). "Chitinase 3
665 like 1 suppresses the stability and activity of p53 to promote lung tumorigenesis." Cell
666 Commun Signal **18**(1): 5.
667 Perez, E., J. L. Lindblad and A. Bergmann (2017). "Tumor-promoting function of apoptotic
668 caspases by an amplification loop involving ROS, macrophages and JNK in Drosophila."
669 Elife **6**.
670 Perkins, K. K., G. M. Dailey and R. Tjian (1988). "Novel Jun- and Fos-related proteins in
671 Drosophila are functionally homologous to enhancer factor AP-1." EMBO J **7**(13): 4265-
672 4273.
673 Pesch, Y. Y., D. Riedel, K. R. Patil, G. Loch and M. Behr (2016). "Chitinases and Imaginal
674 disc growth factors organize the extracellular matrix formation at barrier tissues in insects."
675 Sci Rep **6**: 18340.
676 Pinder, J. C., D. Bray and W. B. Gratzer (1975). "Actin polymerisation induced by spectrin."
677 Nature **258**(5537): 765-766.
678 Pinho, A. V., L. Chantrill and I. Rooman (2014). "Chronic pancreatitis: a path to pancreatic
679 cancer." Cancer Lett **345**(2): 203-209.
680 Recouvreux, M. V. and C. Commisso (2017). "Macropinocytosis: A Metabolic Adaptation to
681 Nutrient Stress in Cancer." Front Endocrinol (Lausanne) **8**: 261.
682 Roslind, A. and J. S. Johansen (2009). "YKL-40: a novel marker shared by chronic
683 inflammation and oncogenic transformation." Methods Mol Biol **511**: 159-184.
684 Shao, R., K. Hamel, L. Petersen, Q. J. Cao, R. B. Arenas, C. Bigelow, B. Bentley and W. Yan
685 (2009). "YKL-40, a secreted glycoprotein, promotes tumor angiogenesis." Oncogene **28**(50):
686 4456-4468.
687 Tang, H., Y. Sun, Z. Shi, H. Huang, Z. Fang, J. Chen, Q. Xiu and B. Li (2013). "YKL-40
688 induces IL-8 expression from bronchial epithelium via MAPK (JNK and ERK) and NF-
689 kappaB pathways, causing bronchial smooth muscle proliferation and migration." J Immunol
690 **190**(1): 438-446.
691 Tjota, M., S. K. Lee, J. Wu, J. A. Williams, M. R. Khanna and G. H. Thomas (2011). "Annexin
692 B9 binds to beta(H)-spectrin and is required for multivesicular body function in Drosophila."
693 J Cell Sci **124**(Pt 17): 2914-2926.
694 Tran, D. T. and K. G. Ten Hagen (2017). "Real-time insights into regulated exocytosis." J Cell
695 Sci **130**(8): 1355-1363.

696 Uhlen, M., C. Zhang, S. Lee, E. Sjostedt, L. Fagerberg, G. Bidkhori, R. Benfeitas, M. Arif, Z.
697 Liu, F. Edfors, K. Sanli, K. von Feilitzen, P. Oksvold, E. Lundberg, S. Hober, P. Nilsson, J.
698 Mattsson, J. M. Schwenk, H. Brunnstrom, B. Glimelius, T. Sjoblom, P. H. Edqvist, D.
699 Djureinovic, P. Micke, C. Lindskog, A. Mardinoglu and F. Ponten (2017). "A pathology
700 atlas of the human cancer transcriptome." Science **357**(6352).
701 Wertheimer, E., A. Gutierrez-Uzquiza, C. Rosemblit, C. Lopez-Haber, M. S. Sosa and M. G.
702 Kazanietz (2012). "Rac signaling in breast cancer: a tale of GEFs and GAPs." Cell Signal
703 **24**(2): 353-362.
704 Williams, S. T., A. N. Smith, C. D. Cianci, J. S. Morrow and T. L. Brown (2003). "Identification
705 of the primary caspase 3 cleavage site in alpha II-spectrin during apoptosis." Apoptosis **8**(4):
706 353-361.
707 Wu, C., C. Chen, J. Dai, F. Zhang, Y. Chen, W. Li, J. C. Pastor-Pareja and L. Xue (2015). "Toll
708 pathway modulates TNF-induced JNK-dependent cell death in Drosophila." Open Biol **5**(7):
709 140171.
710 Yadav, S. and I. Eleftherianos (2018). "The Imaginal Disc Growth Factors 2 and 3 participate
711 in the Drosophila response to nematode infection." Parasite Immunol **40**(10): e12581.
712 Yang, P., Y. Yang, P. Sun, Y. Tian, F. Gao, C. Wang, T. Zong, M. Li, Y. Zhang, T. Yu and Z.
713 Jiang (2021). "betaII spectrin (SPTBN1): biological function and clinical potential in cancer
714 and other diseases." Int J Biol Sci **17**(1): 32-49.
715 Yeh, Y. T., M. F. Hou, Y. F. Chung, Y. J. Chen, S. F. Yang, D. C. Chen, J. H. Su and S. S.
716 Yuan (2006). "Decreased expression of phosphorylated JNK in breast infiltrating ductal
717 carcinoma is associated with a better overall survival." Int J Cancer **118**(11): 2678-2684.
718 Zeke, A., M. Misheva, A. Remenyi and M. A. Bogoyevitch (2016). "JNK Signaling: Regulation
719 and Functions Based on Complex Protein-Protein Partnerships." Microbiol Mol Biol Rev
720 **80**(3): 793-835.
721 Zhao, T., Z. Su, Y. Li, X. Zhang and Q. You (2020). "Chitinase-3 like-protein-1 function and
722 its role in diseases." Signal Transduct Target Ther **5**(1): 201.
723 Zhu, M., T. Xin, S. Weng, Y. Gao, Y. Zhang, Q. Li and M. Li (2010). "Activation of JNK
724 signaling links lgl mutations to disruption of the cell polarity and epithelial organization in
725 Drosophila imaginal discs." Cell Res **20**(2): 242-245.
726 Ziemnicka-Kotula, D., J. Xu, H. Gu, A. Potempska, K. S. Kim, E. C. Jenkins, E. Trenkner and
727 L. Kotula (1998). "Identification of a candidate human spectrin Src homology 3 domain-
728 binding protein suggests a general mechanism of association of tyrosine kinases with the
729 spectrin-based membrane skeleton." J Biol Chem **273**(22): 13681-13692.

730